scientific reports

OPEN

Four-step eco-friendly energy efficient recycling of contaminated $Nd_2Fe_{14}B$ sludge and coercivity enhancement by reducing oxygen content

Syed Kamran Haider[1,2,3], Dongsoo Kim[1,2✉] & Young Soo Kang[3✉]

Complete recycling of $Nd_2Fe_{14}B$ sludge by chemical methods has gained significance in recent years, however, it is not easy to recycle highly contaminant sludge and obtain product with good magnetic properties. Herein we report a simple four-step process to recycle the $Nd_2Fe_{14}B$ sludge containing ~ 10% of contaminants. Sludge was leached in H_2SO_4 and selectively co-precipitated in two steps. In the first co-precipitation, Al^{3+} and Cu^{2+} were removed at pH 6. Thereafter, in the second co-precipitation Fe^{2+} and RE^{3+} sulfates were converted to the Fe and RE hydroxides. By annealing at 800 °C RE and Fe hydroxides precipitates were converted to the oxides and residual carbon was oxidized to CO_2. After the addition of boric acid, Fe and RE oxides were reduced and diffused to the $(Nd-RE)_2Fe_{14}B$ by calciothermic reduction diffusion. Removal of CaO by washing with D.I. water in glove box reduced the oxygen content (~ 0.7%), improved crystallinity and enhanced the magnetic properties significantly. Coercivity increased more than three times (from 242.71 to 800.55 kA/m) and M_r value was also enhanced up to more than 20% (from 0.481 to 0.605 T). In this green process Na_2SO_4 and $Ca(OH)_2$ were produced as by-product those are non-hazardous and were removed conveniently.

Among permanent magnets, $Nd_2Fe_{14}B$ type hard magnets exhibit the highest recorded BH_{max}[1–5]. They have drawn attention due to their applications in modern appliances which lead to large market demand and a rapid increase in their production[6–11]. A huge amount (21%) of rare earth elements (RE) are being consumed for the synthesis of permanent magnets. RE resources are depleting and the cost of RE extraction from the ores is continuously soaring, hence recycling of the $Nd_2Fe_{14}B$ sludge is becoming an important area of modern research.

A large quantity (~ 30%) of the $Nd_2Fe_{14}B$ sludge is produced in the cutting and grinding process and more than 95 wt% of it, is recyclable[12]. However, because of costly physical recycling processes and high level of contamination, usually, recycling magnet sludge is not economically feasible in most part of the world. $Nd_2Fe_{14}B$ sludge mainly consists of oxidized particles of $Nd_2Fe_{14}B$ with different RE, C, Al, and d-block transition metals (e.g. Cu, Co, Zn, Mn, Cr, Ni). Al, Zn, Mn, Cr, and Ni come from the protective coatings, those are applied to avoid the corrosion of bulk magnet surface. Cu is added to the sintered $Nd_2Fe_{14}B$ magnets to decouple the magnetic grains to stop the fast flip-over of the magnetic domains and enhance the coercivity[11]. Co addition to enhances the M_r value and curie temperature. Sludge can have a high quantity of carbon because of the mixing of machine oil and lubricant during the cutting process. All these contaminants reduce the value of sludge.

Commonly used physical method for recycling of $Nd_2Fe_{14}B$ sludge is a multi-step process which requires a huge amount of chemicals, energy, and produces hazardous wastes as byproduct[13]. These wastes include oxides (of carbon, sulfur, and nitrogen), dangerous metals (e.g. As), organic solvents, RE vapors and electrolytes. Several chemical methods have been introduced for the recovery of RE from $Nd_2Fe_{14}B$ magnets scrap/sludge[12–26] but complete recycling of $Nd_2Fe_{14}B$, via chemical route is relatively new field. Haider et al.[12] and Yin et al.[13] have recently introduced chemical methods. These methods are very innovative and useful, but they deal with sludge

[1]Convergence Research Center for Development of Mineral Resources, Korea Institute of Geoscience and Mineral Resources, 124, Gwahakro, Yuseonggu, Daejeon 34132, Korea. [2]Powder and Ceramics Division, Korea Institute of Materials Science, 797, Changwondaero, Seongsangu, Changwon, Gyeongnam 51508, Korea. [3]Department of Chemistry, Sogang University, 35, Baekbeomro, Mapogu, Seoul 04107, Korea. ✉email: dskim69@kigam.re.kr; yskang@sogang.ac.kr
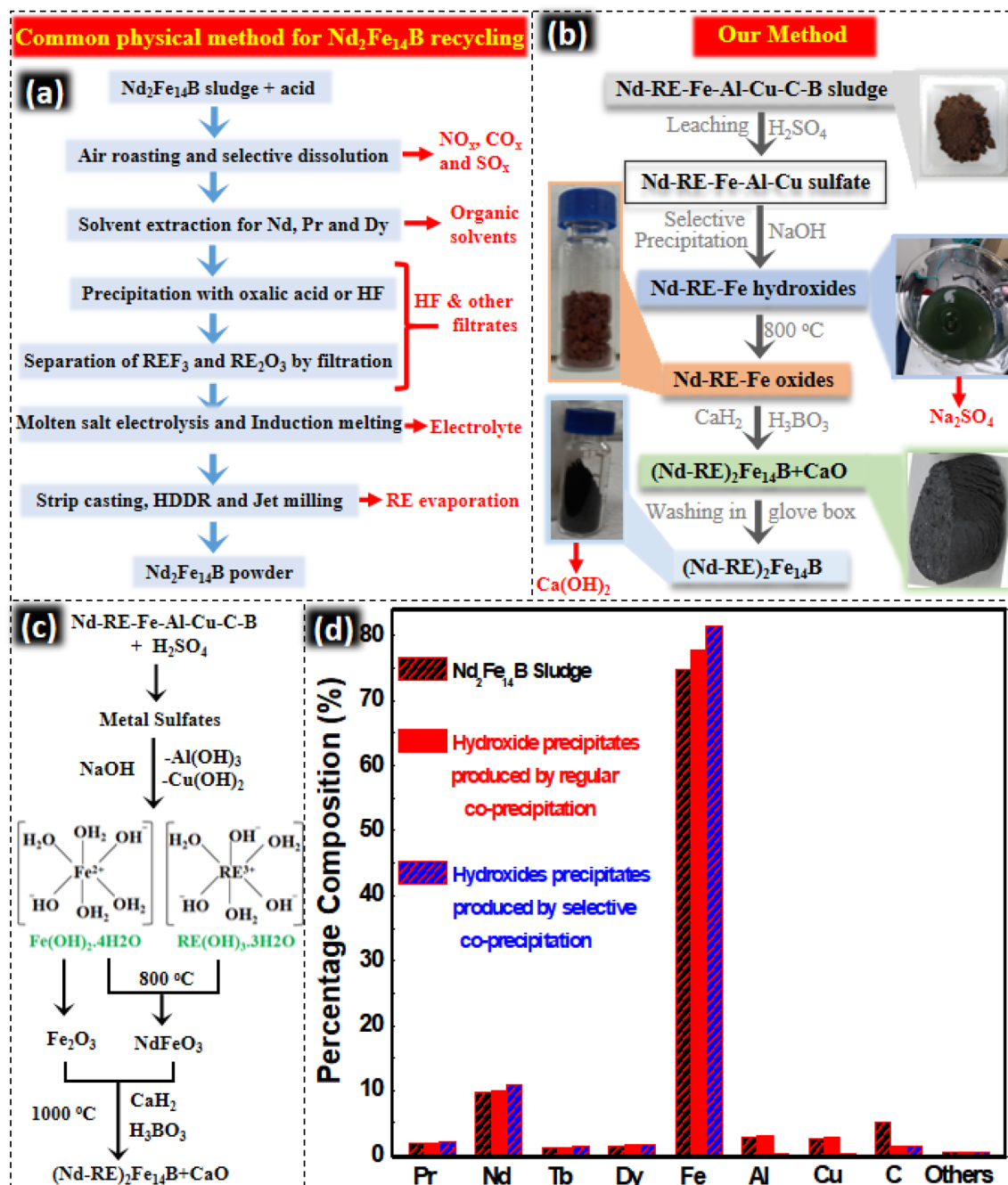
Figure 1. (a) Common physico-chemical method for the recycling of $Nd_2Fe_{14}B$ sludge used these days[12]. (b) Our experimental process. Waste products produced in both methods are shown in red color. (c) Chemistry of the process. (d) Composition of the sludge and hydroxides precipitates produced after regular and selective co-precipitation.

with a low level of contamination. It is very difficult to control the contamination in the sludge, hence it was required to introduce a new method to recycle this kind of sludge with good magnetic properties.

Herein we propose a time and energy efficient-recycling method for recycling of $Nd_2Fe_{14}B$ sludge which is equally useful for sludge with high contamination and variable composition. Na_2SO_4 and $Ca(OH)_2$ are produced as byproducts, those are non-hazardous and easy to remove. Magnetic properties are further enhanced by the removal of contamination and reduction of oxygen content. A comparison of between our method and the common physico-chemical[12] method used for the recycling of $Nd_2Fe_{14}B$ sludge is given in the Fig. 1a, b.

Experimental section

Materials. All chemicals used in this work, including neodymium (III) chloride hexahydrate ($Nd_2(SO_4)_3 \cdot 6H_2O$), sodium hydroxide (NaOH), boric acid (H_3BO_3), calcium hydride (CaH_2), sulfuric acid (H_2SO_4), ethyl alcohol (C_2H_5OH) and acetone (CH_3COCH_3) were analytical grade and obtained from Sigma-Aldrich Co. Magnet sludge was obtained during the cutting process of $Nd_2Fe_{14}B$.

Experimental process. Magnet sludge obtained during the cutting of $Nd_2Fe_{14}B$ magnet was dissolved in 2M H_2SO_4 by leaching process. ICP analysis (by inductively coupled plasma atomic emission spectrometer) of the leachate showed that it consisted of Nd, Pr, Tb, Fe, Cu, Al, and C (Fig. 1a). Total RE:Fe molar ratio in the leachate was calculated as 15.8:83.8. In order to compensate for the lower RE concentration in the leachate and to make up the RE:Fe molar ratio as 15:77, extra $Nd_2(SO_4)_3 \cdot 6H_2O$ was added to the leachate solution.

Co-precipitation of leachate was performed with a 3.5M NaOH solution which was added drop-by-drop, to raise the pH of the leachate solution up to 6. At pH 6, Al, Zn, and Cu chlorides were converted to their respective hydroxide precipitates. These precipitates were removed from the reaction mixture by centrifugation. The left-over reaction mixture was co-precipitated by further addition of NaOH solution. By maintaining the pH at 13, the solution was stirred for 30 min, which lead to the formation of RE and Fe hydroxides precipitates. The precipitates were washed thrice with de-ionized water to remove the Na_2SO_4 and NaOH and then annealed at 800 °C to convert all Fe and RE hydroxides to oxides. The annealing was done for 30 min while the air was flowing in the furnace. Produced oxide particles were mixed with boric acid and CaH_2 in glove box and the mixture was pressed to the pellet. Pellet increases the physical contact between the constituents e.g. calcium hydride, boric acid, oxides of RE and Fe, which is useful for the efficient R-D (reduction-diffusion). Boric acid was added in such a way that the molar ratio of RE:Fe:B was kept as 15:77:8. Oxides (+ boric acid):CaH_2 weight ratio was fixed as 1:1.

RE and Fe oxides (mixed with CaH_2) were reduced and diffused by annealing at 1000 °C for 3 h. Products obtained after R-D were washed with water in the glove box repeatedly to remove CaO and rinsed with acetone twice. Finally, vacuum drying was done and recycled (Nd-RE)$_2$Fe$_{14}$B powder was stored in inert conditions. Flow diagram of experimental process and summary of chemical reactions during the process are provided as Fig. 1b, c. Advantages (energy efficient and cost effective) of the chemical method over the commonly used method are described in the Figs. S1 and S2, in the supporting information.

Characterization. The concentration of the elements in the leachate was determined by the inductively coupled plasma atomic emission spectrometer (ICP-AES, Shimadzu). Crystal structure and phases were determined by X-ray diffraction (XRD) patterns using a Rigaku Diffractometer (XRD, Rigaku). The morphology, size, and elemental distribution were observed with field emission scanning electron microscope (FE-SEM, Merlin), conventional transmission electron microscopy (TEM, JEM-2100F), and aberration-corrected TEM (ARM-200F) with energy-dispersive X-ray spectroscopy (EDS). TEM was operated at the accelerating voltage of 200 kV. Magnetic properties (M-H curves) of final product were measured by Physical Property Measurement System (PPMS, Evercool II–9T) in the vibrating sample magnetometer mode. LECO ON-736 analyzer was used to determine the oxygen content in (Nd-RE)$_2$Fe$_{14}$B.

Specimens for TEM were prepared by focused ion beam (FIB- NX2000, Hitachi) using the lift-out technique. For TEM measurement, the sample was treated as the same process reported by Kim et al.[27] and orientation of the sample along the required zone axis was confirmed by using electron backscatter diffraction (EBSD) by TEAM™ Pegasus, Ametek Co. Ltd. USA.

Results and discussion

Magnet sludge produced during the cutting of $Nd_2Fe_{14}B$ was dissolved in the H_2SO_4. Overall composition of the sludge before and after the precipitation is provided in Fig. 1d. Sludge mainly consisted of RE (Nd, Pr, Tb, Dy) Fe, Cu, Al, and C. Traces of other elements (e.g. Ho, Zr, Ga, Ni, Co) were also detected in the ICP analysis but their total concentration was ~ 0.4%. Effect of these small impurities on the magnetic properties of the final product was studied and provided in the supporting information. Cu, Al and C were ~ 10% those could significantly reduce the magnetic properties of the (Nd-RE)$_2$Fe$_{14}$B produced from them. After leaching of sludge in the H_2SO_4, next step was the selective precipitation to remove Al^{3+} and Cu^{2+}. Precipitation of multivalent (e.g. Al^{3+} and Cu^{2+}) ions from the solution depends on many factors e.g. oxidation state, Ksp value, the concentration of other ions, precipitating agent, and temperature. Precipitation of Fe^{3+}, Al^{3+}, and Cu^{2+} from their chloride solution occurred at pH values of 3.5, 5.0, and 6.0[28]. However, different results were observed, when the solution of acid mine drainage containing Fe^{3+}, Al^{3+}, and Cu^{2+} was co-precipitated[28]. In the acid mine drainage experiment, Fe^{3+}, Al^{3+}, and Cu^{2+} chlorides were precipitated at pH 3.5, 4.5, and 5.5, respectively[28]. Precipitation of Al^{3+} and Cu^{2+} at pH value of 5.5 was also observed[29]. Different pH of the precipitation for Al^{3+} and Cu^{2+} in the previous studies indicated is a complicated process. It is commonly observed that Fe^{3+} precipitates completely at pH value ~ 3, however, Fe^{2+} precipitates at pH value of ~ 7[30]. In our study, when pH approached 4, Al (Ksp constant = 1.9×10^{-33}) started to precipitate.

Ksp constants of Cu(OH)$_2$ is 1.6×10^{-19} and it was next to be precipitated hence precipitated out between the pH values of 5–6. Almost ~ 90% hydroxides of Al and Cu were separated in the form of precipitates at pH 6, they were removed from the leachate solution by centrifugation. Separated Al and Cu hydroxides were analyzed, and analysis details are provided in the supporting information (Figs. S3, S4).

Fe in the leachate exists as Fe^{2+} which does not precipitate below pH 6 but slightly (~ 2%) precipitates at pH 6 (Fig. S5). However, when pH value exceeded 6, Fe^{2+} (Ksp constant = 7.9×10^{-15}) started to precipitate as Fe(OH)$_2$. Soe et al.[31] reported that Nd^{3+}, Pr^{3+}, Dy^{3+}, and Tb^{3+} also start to precipitate at pH value of ~ 7 and similar was observed in our study.
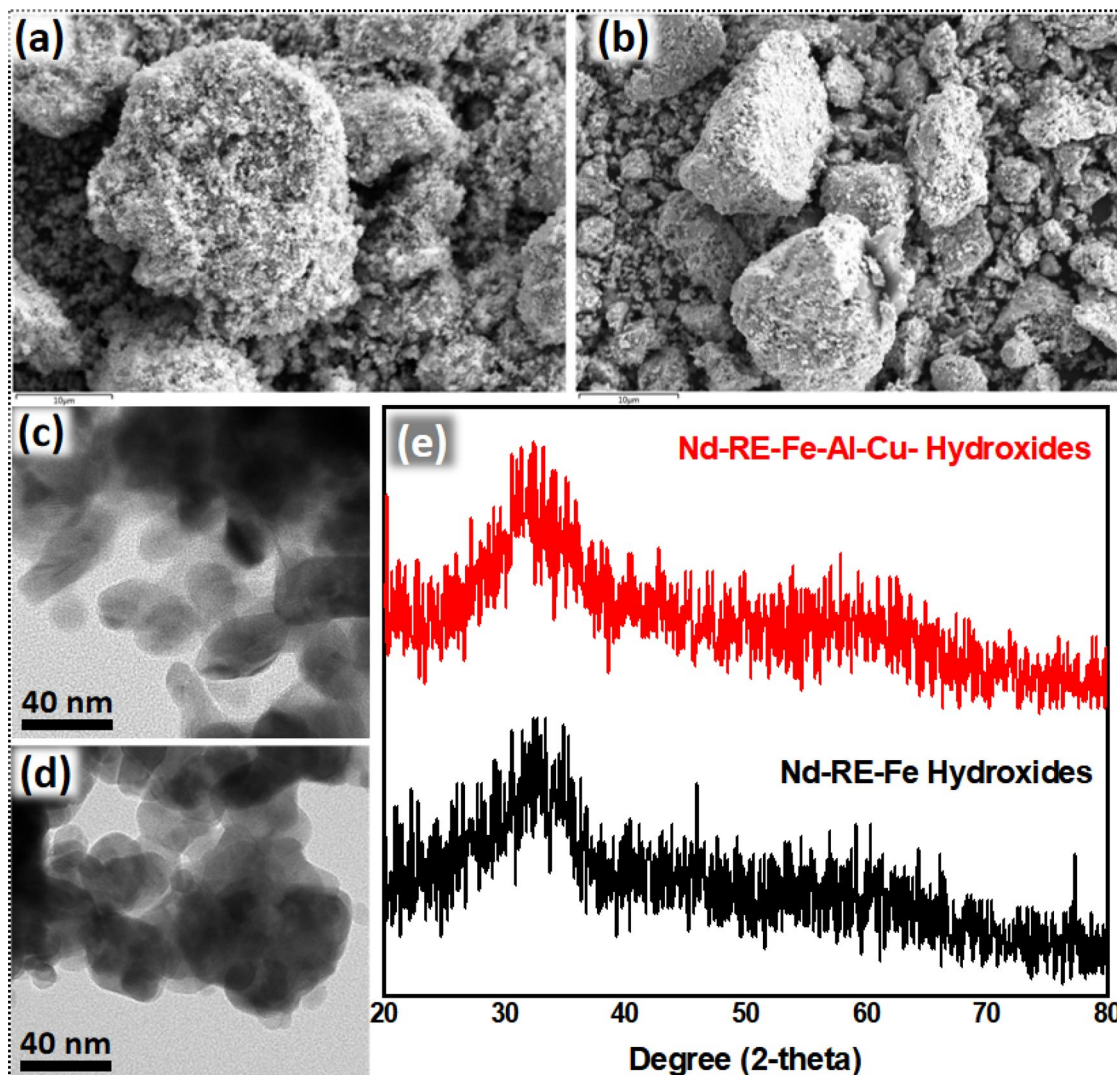
Figure 2. SEM image of hydroxide precipitates of (**a**) Nd-RE-Fe-Al-Cu and (**b**) Nd-RE-Fe. TEM image of hydroxide precipitates of (**c**) Nd-RE-Fe-Al-Cu and (**d**) Nd-RE-Fe. (**e**) XRD patterns of Nd-RE-Fe-Al-Cu and Nd-RE-Fe hydroxide precipitates.

Co-precipitation was stopped at pH values of 10, 11, 12 and 13 in four different experiments. The maximum percentage yield was obtained at pH value of 13 (Fig. S6). At pH 13, a mixture of hydroxides of RE, and Fe, was obtained with traces of some impurities e.g. Cu, Al, Ho, Zr, Ga, Ni, Co (less than 1%). In a separate experiment, selective precipitation was not performed and all the elements in the leachate solution were co-precipitated, hence, a mixture of RE, Fe, Al, and Cu hydroxide was obtained.

Hydroxides obtained by co-precipitation were aqua complexes of RE and other metals. Being amorphous, these hydroxides could not be detected by XRD (Fig. 2e) analysis. SEM image of the hydroxide precipitates produced by regular and selective co-precipitation (Fig. 2a, b) confirmed that hydroxide particles were of irregular morphology and size (Fig. 2c, d). TEM analysis revealed that the average size of the hydroxide precipitates was ~ 25 nm. TEM-EDS images (Figs. S7, S8) confirmed that oxides of all the metals are homogeneously mixed.

Most of the carbon was removed during the precipitation and centrifugation but still, noticeable quantity was detected in the hydroxide precipitates (Fig. 1d). Leftover carbon was removed by the annealing in air at 800 °C. Oxidation at 800 °C converted all the C to CO_2. Meanwhile, annealing also converted hydroxide precipitates to the oxides. SEM analysis revealed that the average particle size of the oxide particles was ~ 150 nm (Fig. 3a, b).

XRD confirmed the presence of Fe_2O_3 and $REFeO_3$ phases in the oxide mixture (Fig. 3m). The mechanism of formation of these oxides is given in Fig. 1c. Peaks of Cu and Al oxides were also observed in the XRD patterns of oxides produced from Nd, RE, Fe, Al, Cu hydroxide precipitates. TEM-EDS images reveal that all RE, Fe, Cu, and Al are distributed evenly throughout the oxide intermediates (Fig. 3c–l). Co-precipitation brought the Fe_2O_3 and $REFeO_3$ particles very close. This homogeneous distribution is very effective for the efficient reduction diffusion process. Oxides produced from both the selective and regular co-precipitation were mixed with the boric acid and CaH_2 in two separate experiments. These mixtures were reduced and diffused at 1000 °C to obtain $(Nd-RE)_2Fe_{14}(AlCu)B$ and $(Nd-RE)_2Fe_{14}B$. Both of these products contained CaO byproduct, and were
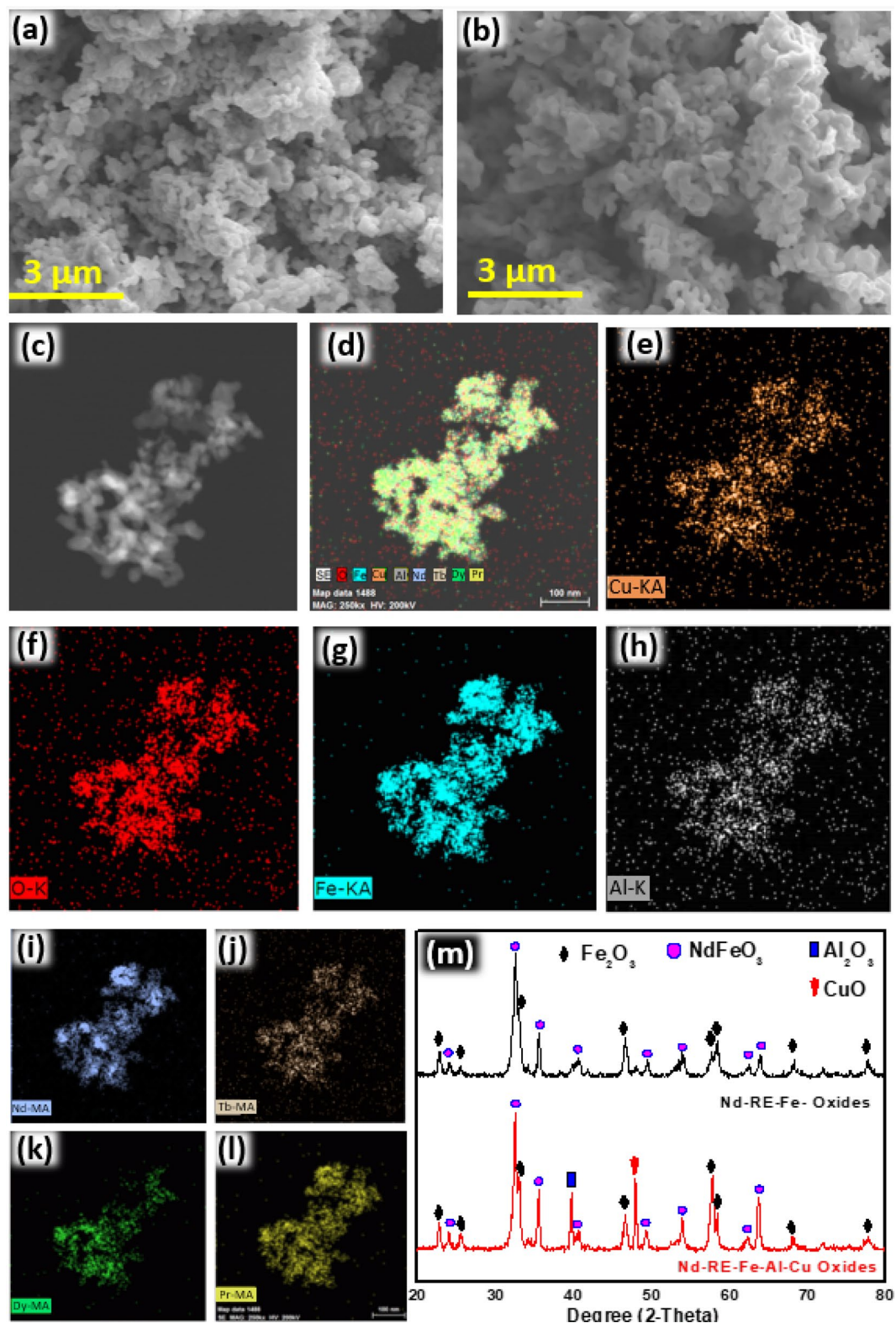
Figure 3. SEM images of (**a**) Nd-RE-Fe-oxide (**b**) Nd-RE-Fe-Al-Cu-oxide (**c–l**) TEM and TEM-EDS images of Nd-RE-Fe-Al-Cu-oxide (**m**) XRD patterns of Nd-RE-Fe-oxide and Nd-RE-Fe-Al-Cu-oxide.
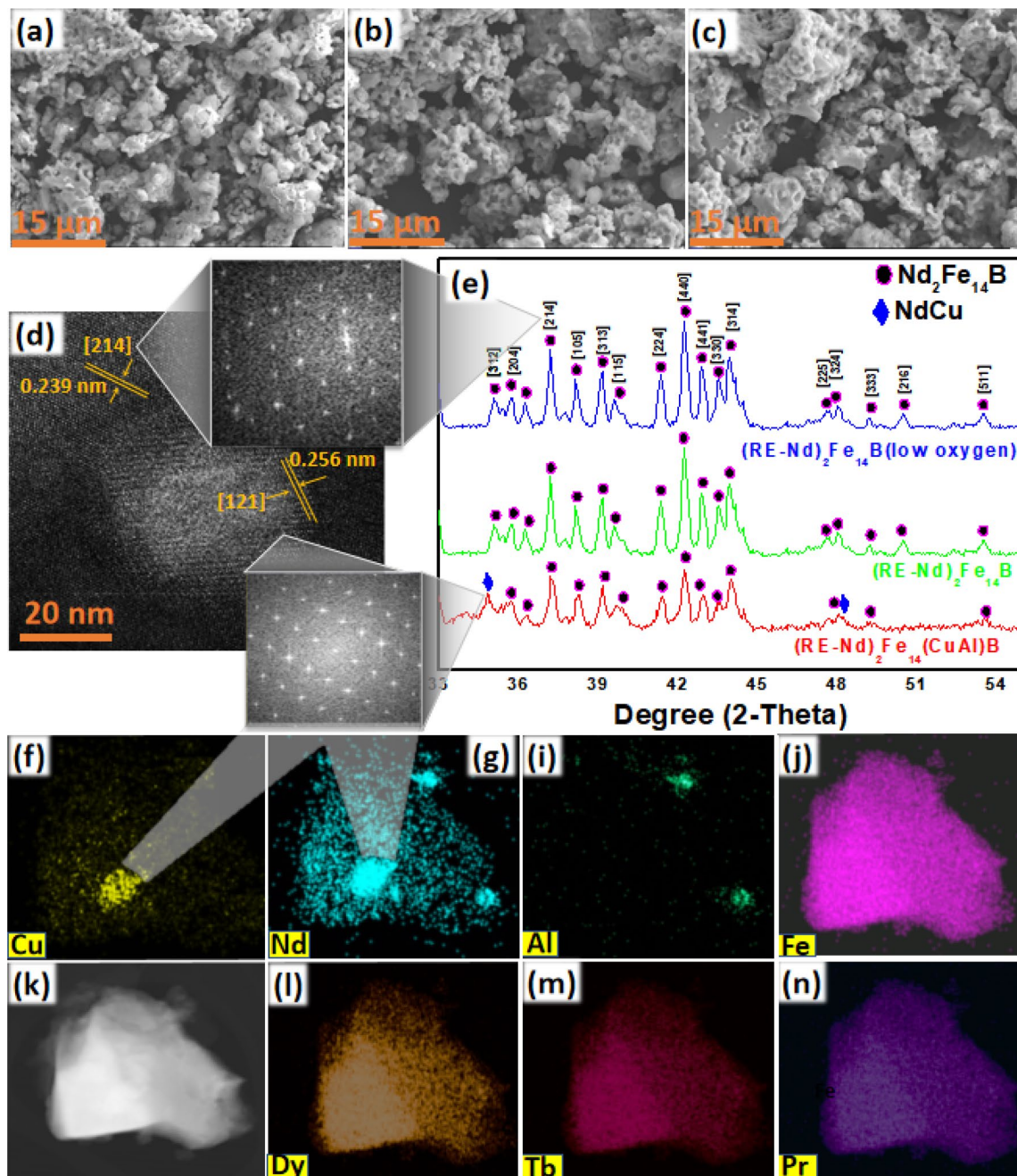
Figure 4. SEM images of (**a**) (Nd-RE)$_2$Fe$_{14}$(AlCu)B, (**b**) (Nd-RE)$_2$Fe$_{14}$B, (**c**) (Nd-RE)$_2$Fe$_{14}$B-(low oxygen), (**d**) HRTEM and SEAD patterns of (Nd-RE)$_2$Fe$_{14}$(AlCu)B, (**e**) XRD patterns for all three products, (**f–n**) TEM-EDS images of (Nd-RE)$_2$Fe$_{14}$(AlCu)B.

washed with water to remove it. (Nd-RE)$_2$Fe$_{14}$(AlCu)B was washed in the air while (Nd-RE)$_2$Fe$_{14}$B was divided into two parts. One part was washed in the air and other part was washed in the glove box to minimize the exposure to oxygen. In this way three different products (Nd-RE)$_2$Fe$_{14}$(AlCu)B, (Nd-RE)$_2$Fe$_{14}$B and (Nd-RE)$_2$Fe$_{14}$B (low oxygen), were obtained. To determine the detailed structure of the products XRD, SEM, SEM–EDS, TEM, TEM-EDS, and HRTEM analysis were performed. Nd$_2$Fe$_{14}$B, Dy$_2$Fe$_{14}$B, Tb$_2$Fe$_{14}$B, and Pr$_2$Fe$_{14}$B have similar crystal structures, hence their XRD patterns are also very similar. It was very hard to distinguish between all four RE$_2$Fe$_{14}$B phases with the help of XRD. Hence all these phases are marked as Nd$_2$Fe$_{14}$B (JCPSD #36-1296) in the XRD patterns shown in Fig. 4e. NdCu (JCPSD #337-1037) phase was also detected in the XRD analysis of (Nd-RE)$_2$Fe$_{14}$(AlCu)B. To evaluate the crystallinity of the of (Nd-RE)$_2$Fe$_{14}$(AlCu)B, SAED patterns (Fig. 3b) of the Nd$_2$Fe$_{14}$B and ZnCu were obtained. With d-spacing value of 0.239 nm, [214] facet of (Nd-RE)$_2$Fe$_{14}$B was detected. Any peak of Al or Al alloy was not detected in the XRD, however, in TEM-EDS image, Al was detectable (Fig. 4i). This may refer to that Al or Al alloy was not crystallized well during reduction-diffusion or maybe oxidized during the washing with water and became amorphous. However, [121] facet of NdCu was identified in the HRTEM with the d-spacing value of 0.256 nm (Fig. 4d).

SEM images in Fig. 4a–c revealed that the magnetic particles had irregular morphology and the size varied from 0.3 to 10 μm. It was determined that the average particle size of all three particles was ~ 1.8 μm (Fig. 4a–c). Different studies have revealed that Dy, Pr Tb, and other heavy RE are substituted inside the $Nd_2Fe_{14}B$ crystal lattice[32–43]. In our study HRTEM and SEM–EDS images (Fig. 4l–n) also confirmed it. HRTEM shows that the crystal lattice d-spacing at [214] facet is 0.239 nm, which is slightly smaller (241 nm) than $NdFe_{14}B$ [214] facet. Slight reduction in the d-spacing may also indicate the substitution of Pr, Tb, or Dy in the crystal lattice. TEM-EDS images of $(Nd-RE)_2Fe_{14}(AlCu)B$ confirmed the homogeneous mixing of all RE, indicate the substitution of Dy, Pr, and Tb in the $Nd_2Fe_{14}B$ crystal lattice (Fig. 4f–n). TEM and TEM-EDS images of $(Nd-RE)_2Fe_{14}B$ and $(Nd-RE)_2Fe_{14}B$ (low oxygen) are provided in supporting information as Figs. S9, S10 and S11.

Oxygen content in the commercial $(Nd-RE)_2Fe_{14}B$ powders is ~ 0.4%. This one of the reasons that commercial $(Nd-RE)_2Fe_{14}B$ powders exhibit excellent magnetic properties. In the rare earth based magnetic particles produced by the R-D, washing with the water is employed to remove the CaO, byproduct of the R-D process[44]. On average, $(Nd-RE)_2Fe_{14}B$ magnetic particles produced by the reduction diffusion process contains ~ 2% of oxygen. It was concluded that oxygen content reduces the crystallinity $Nd_2Fe_{14}B$ because no oxide is detected in the XRD patterns. To solve the oxidation problem, $(Nd-RE)_2Fe_{14}B$ was washed in the glove box. Before washing the $(Nd-RE)_2Fe_{14}B$ with the water in the glove box, nitrogen gas was blown in the water, which further removed the dissolved oxygen in the water. N_2 was simply purged into the water at the rate of 25 ml/s for 40 min. This condition was taken from the work by Butler et al.[45] as they have reported that more than 60% of the oxygen can be removed at this optimum condition. The glove box was filled with the Ar, with the oxygen level reduced to the ~ 50 ppm. By taking these preventive measures, the oxygen content of $(Nd-RE)_2Fe_{14}B$ was reduced to ~ 0.7%. Figure 4e shows that the Nd peak is absent when the washed $(Nd-RE)_2Fe_{14}B$ was washed in air. This further confirms that washing with the water reduces the crystallinity of the Nd too. It is well-known fact that the addition of the Nd phase (up to a certain limit) enhances the magnetic properties especially, coercivity[12].

LAADF-STEM images (Fig. 5b–d) were zoomed in to investigate the micro-structure of the magnetic particles. Line EDS mapping from the HAADF-STEM image was taken and studies to determine the degree of oxidation near the grain boundary (Fig. 5e, f). Pr, Dy, and Tb are substituted inside the $(Nd-RE)_2Fe_{14}B$, hence their EDS mapping was not studied to avoid the complexity of data. It was found that oxygen content suddenly increased near the grain boundary because these parts of the grain are directly exposed to the water during the washing process. Pb and Sn detected in TEM-EDS come from the solder.

It is evident from the XRD patterns (Fig. 4e) that Cu and Al reduce the crystallinity of the final product, as well as few crystal facets (e.g. [216],[324]), are also missing. The exact mechanism that how Cu and Al affects the $(Nd-RE)_2Fe_{14}B$ crystal is yet unknown but most probably Cu and Al interfere during the diffusion of RE, Fe, and B. Poor crystallization after reduction-diffusion is the major factor that reduced the magnetic properties of $(Nd-RE)_2Fe_{14}(AlCu)B$. The second reason for the poor magnetic properties of $(Nd-RE)_2Fe_{14}(AlCu)B$ is the non-magnetic behavior of Cu. Cu has an electronic configuration of $[Ar] 3d^{10} 4s^1$ which indicates the absence of unpaired electrons. Hence Cu and its alloys tend to be non-magnetic. In the bulk sintered $(Nd-RE)_2Fe_{14}B$ magnets, Cu is used to decouple the large magnetic grains. Nd-Cu reduces the effect of the surge of domain wall removal in bulk magnets and enhances the coercivity. But in the case of magnetic particles, the grain decoupling phenomenon does not work efficiently. Hence non-magnetic Nd-Cu phase reduces the overall magnetic properties of the $(Nd-RE)_2Fe_{14}(Cu-Al)B$. Al is detectable in the final product but it is in the amorphous form. Effect of amorphous Al or its possible amorphous alloy on the magnetic properties is not clear.

Decreasing order of the Ms value in all the products is given as $(Nd-RE)_2Fe_{14}(AlCu)B > (Nd-RE)_2Fe_{14}B$-(low oxygen) > $(Nd-RE)_2Fe_{14}B$. $(Nd-RE)_2Fe_{14}(AlCu)B$ has highest Ms value, which indicates the presence of amorphous Fe or low anisotropy field. $(Nd-RE)_2Fe_{14}B$-(low oxygen) has slightly higher Ms value as compared to the $(Nd-RE)_2Fe_{14}B$ that refers to the enhanced Mr value of $(Nd-RE)_2Fe_{14}B$-(low oxygen), which slightly affected the Ms. However, this enhancement in the Ms value is much higher as compared to the Ms value, which is also evident in the squareness ratio graph (Fig. 5a) showing the enhanced squareness ratio of $(Nd-RE)_2Fe_{14}B$-(low oxygen).

$(Nd-RE)_2Fe_{14}(AlCu)B$ exhibit the highest magnetic moment (21.6 μB) and M_s (1.057 T) value among all three products. Higher magnetic moment and low M_r value of $(Nd-RE)_2Fe_{14}(AlCu)B$ refer to the low anisotropic field or presence of amorphous soft magnetic phase (e.g. Fe). Higher M_r value of $(Nd-RE)_2Fe_{14}B$-(low oxygen) contributes to its highest squareness ratio among all three products (Fig. 5a). Individual values of magnetic moments of $(Nd-RE)_2Fe_{14}(AlCu)B$, $(Nd-RE)_2Fe_{14}B$, and $(Nd-RE)_2Fe_{14}B$-(low oxygen) were determined as 21.06, 20.5, and 18.4 μB, respectively. These values of magnetic moments were determined by the M_s values from hysteresis loops (Fig. 5a). Complete hysteresis loops with applied magnetic field range of − 9.5 to 9.5 Tesla are provided in supporting information as Fig. S12.

Reduction in magnetic moment enhanced the coercivity. From the hysteresis loops, coercivity values of $(Nd-RE)_2Fe_{14}(AlCu)B$, $(Nd-RE)_2Fe_{14}B$, and $(Nd-RE)_2Fe_{14}B$-(low oxygen) were determined as 242.71, 568.13 and 800.55 kA/m, respectively. $(Nd-RE)_2Fe_{14}B$-(low oxygen) showed the highest coercivity due to low oxygen content, better crystallinity, and least magnetic moment. Oxygen content values of $(Nd-RE)_2Fe_{14}(AlCu)B$, $(Nd-RE)_2Fe_{14}B$ and $(Nd-RE)_2Fe_{14}B$-(low oxygen) are recorded as 2.2, 2.1 and 0.7%. The increasing order of coercivity is $(Nd-RE)_2Fe_{14}(AlCu)B < (Nd-RE)_2Fe_{14}B < (Nd-RE)_2Fe_{14}B$-(low oxygen) and the decreasing order of magnetic moment is $(Nd-RE)_2Fe_{14}(AlCu)B > (Nd-RE)_2Fe_{14}B$-(low oxygen) > $(Nd-RE)_2Fe_{14}B$. Individual M_r values of $(Nd-RE)_2Fe_{14}(AlCu)B$, $(Nd-RE)_2Fe_{14}B$, and $(Nd-RE)_2Fe_{14}B$-(low oxygen) were determined as 0.481, 0.489, 0.605 T, respectively. M_r (emu/g), M_s (emu/g), squareness ratio (S_q), magnetic moment (μB), and coercivity (H_c), for the all the products are shown in Fig. 5a and Table S2, comparatively.
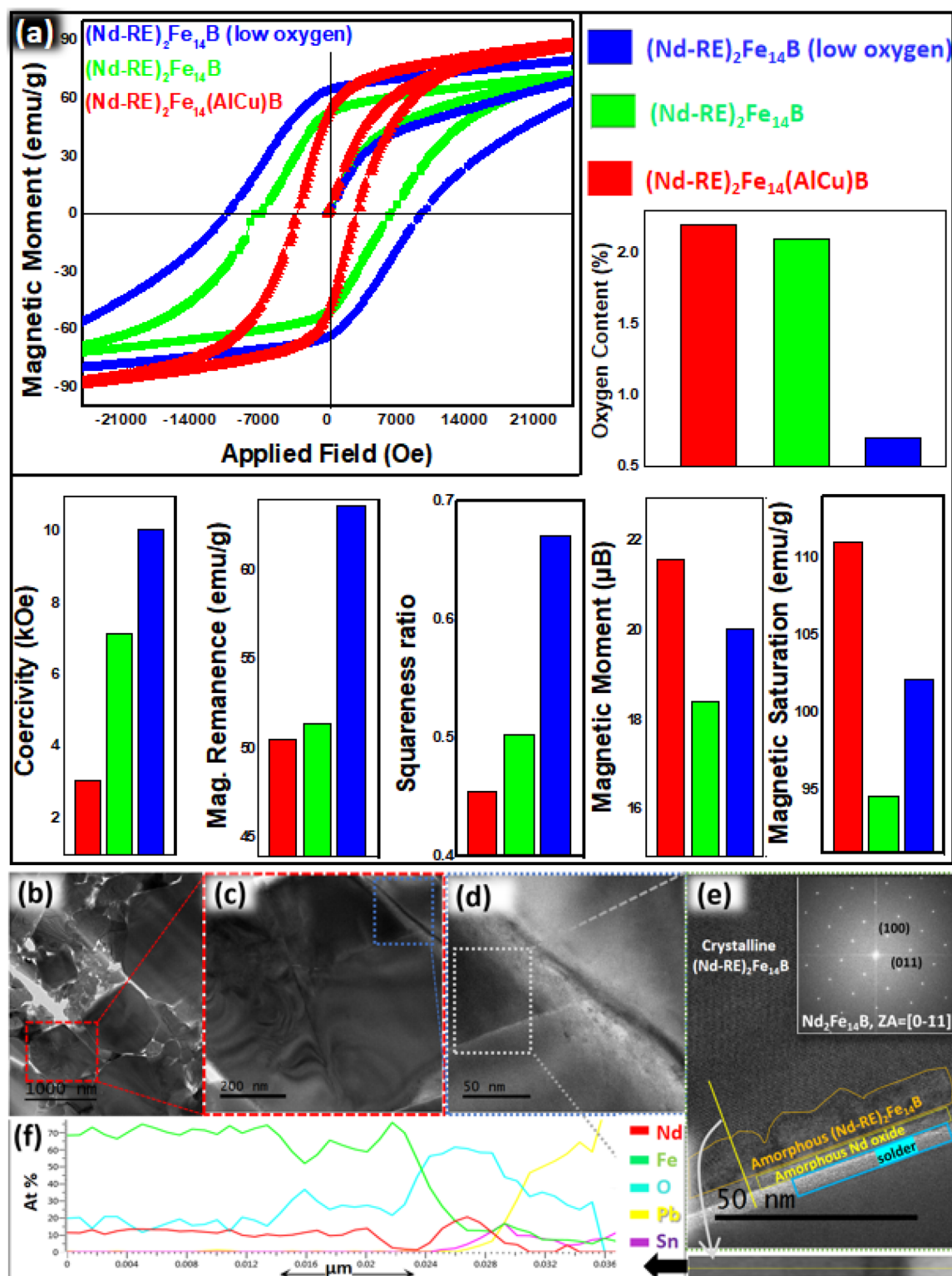
Figure 5. (**a**) Magnetic properties and oxygen content of all products (**b**–**d**) LAADF-STEM image of $Nd_2Fe_{14}B$ (**e**) HAADF-STEM image from (**d**) (**f**) EDS line profile from (**e**).

Conclusion

Contaminated $Nd_2Fe_{14}B$ sludge was recycled by four-step chemical process. The process consisted of leaching of sludge in H_2SO_4, removal of impurities by selective co-precipitation, annealing, and calciothermic reduction diffusion. Al^{3+} and Cu^{3+} were removed by co-precipitation at pH 6 and residual carbon was removed by annealing at 800 °C. CaO byproduct was separated by washing in the glove box, in presence of very low level of oxygen that reduced the oxidation of $(Nd-RE)_2Fe_{14}B$ produced. Removal of impurities and low oxygen content (~ 50 ppm)

tripled the coercivity (over 800 kA/m) and enhanced the M_r value up to 0.605 T. The Method reported in this study is simple, eco-friendly, and energy efficient.

References

1. Muljadia, M. & Sardjonoa, P. Preparation and characterization of 5 wt% epoxy resin bonded magnet NdFeB for micro generator application. *Energy Procedia* **68**, 282–287. https://doi.org/10.1016/j.egypro.2015.03.257 (2015).
2. Honshima, M. & Ohashi, K. High-Energy NdFeB agnets and their applications. *J. Mat. Eng. Perform.* **3**(2), 218–222. https://doi.org/10.1007/BF02645846 (1994).
3. Ma, X. H. *et al.* Preparation of Nd–Fe–B by nitrate–citrate auto-combustion followed by the reduction–diffusion process. *Nanoscale* **7**, 8016–8022. https://doi.org/10.1039/C5NR01195G (2015).
4. Jeong, H. *et al.* Chemical synthesis of $Nd_2Fe_{14}B$ hard phase magnetic nanoparticles with an enhanced coercivity value: effect of CaH_2 amount on the magnetic properties. *New J. Chem.* **40**, 10181. https://doi.org/10.1039/C6NJ02436J (2016).
5. Kim, C. W., Kim, Y. H., Pal, U. & Kang, Y. S. Facile synthesis and magnetic phase transformation of Nd–Fe–B nanoclusters by oxygen bridging. *J. Mater. Chem. C* **1**, 27. https://doi.org/10.1039/C2TC00083K (2013).
6. Amirouche, F., Zhou, Y. & Johnson, T. Current micro pump technologies and their biomedical applications. *Microsyst. Technol.* **15**, 647–666. https://doi.org/10.1007/s00542-009-0804-7 (2009).
7. Chen, Z., Miller, D. & Herchenroeder, J. High performance nanostructured Nd–Fe–B fine powder prepared by melt spinning and jet milling. *J. Appl. Phys.* **107**, 09A730.1–0A7303.4. https://doi.org/10.1063/1.3348544 (2010).
8. Riaño, S. & Binnemans, K. Extraction and separation of neodymium and dysprosium from used NdFeB magnets: an application of ionic liquids in solvent extraction towards the recycling of magnets. *Green Chem.* **17**, 2931–2942. https://doi.org/10.1039/C5GC00230C (2015).
9. Reimer, M. V., Schenk-Mathes, H. Y., Hoffmann, M. F. & Elwert, F. Recycling decisions in 2020, 2030, and 2040, when can substantial NdFeB extraction be expected in the EU?. *Metals* **8**, 867.1-867.5. https://doi.org/10.3390/met8110867 (2018).
10. Cha, H. G., Kim, Y. H., Kim, C. W. & Kang, Y. S. Preparation for exchange-coupled permanent magnetic composite between α-Fe (soft) and Nd2Fe14B (hard). *Curr. Appl. Phys.* **7**(4), 400–403. https://doi.org/10.1016/j.cap.2006.09.010 (2007).
11. Akiya, T., Kato, H., Sagawa, M. & Koyama, K. Enhancement of coercivity in Al and Cu added Nd-Fe-B sintered magnets by high field annealing. *IOP Conf. Ser. Mat. Sci. Eng.* https://doi.org/10.1088/1757-8981/1/1/012034 (2009).
12. Syed, K. H., Jin-Young, L., Dongsoo, K. & Kang, Y. S. Eco-friendly facile three-step recycling method of (Nd-RE)$_2$Fe$_{14}$B magnet sludge and enhancement of (BH)max by ball milling in ethanol. *ACS Sustain. Chem. Eng.* **8**, 8156–8163. https://doi.org/10.1021/acssuschemeng.0c00584 (2020).
13. Yin, X. *et al.* Recycled Nd-Fe-B sintered magnets prepared from sludges by calcium reduction-diffusion process. *J. Rare Earth* **36**, 1284–1291. https://doi.org/10.1016/j.jre.2018.03.028 (2018).
14. Saguchi, A., Asabe, K., Takahashi, W., Suzuki, R. O. & Ono, K. Recycling of rare earth magnet scrap, Part 3 carbon removal from Nd magnet grinding sludge under vacuum heating. *Mater. Trans.* **43**, 256–260. https://doi.org/10.2320/matertrans.43.256 (2002).
15. Asabe, K., Saguchi, A., Takahashi, W., Suzuki, R. O. & Ono, K. Recycling of rare earth magnet scrap: part 1 carbon removal by high temperature oxidation. *Mater. Trans.* **42**, 2487–3249. https://doi.org/10.2320/matertrans.42.2487 (2001).
16. Saito, T., Sato, H., Ozawa, S., Yu, J. & Motegi, T. The extraction of Nd from waste Nd–Fe–B alloys by the glass slag method. *J. Alloys Compd.* **353**, 189–193. https://doi.org/10.1016/S0925-8388(02)01202-1 (2003).
17. Takeda, O., Okabe, T. H. & Umetsu, Y. Phase equilibria of the system Fe–Mg–Nd at 1076K. *J. Alloys Compd.* **392**, 206–213. https://doi.org/10.1016/j.jallcom.2004.09.020 (2005).
18. Rabatho, J. P., Tongamp, W., Takasaki, Y., Haga, K. & Shibayama, A. Recovery of Nd and Dy from rare earth magnetic waste sludge by hydrometallurgical process. *J. Mater. Cycles Waste Manag.* **15**, 171–178. https://doi.org/10.1007/s10163-012-0105-6 (2013).
19. Vander Hoogerstraete, T., Blanpain, B., Van Gerven, T. & Binnemans, K. From NdFeB magnets towards the rare-earth oxides: a recycling process consuming only oxalic acid. *RSC Adv.* **4**, 64099–64111. https://doi.org/10.1039/C4RA13787F (2014).
20. Abrahami, S. T., Xiao, Y. & Yang, Y. Rare-earth elements recovery from post-consumer hard-disc drives. *Trans. Inst. Min. Metall. Sect. C* **124**, 106–115. https://doi.org/10.1179/1743285514Y.0000000084 (2015).
21. Lai, W., Liu, M., Li, C., Suo, H. & Yue, M. Recovery of a composite powder from NdFeB slurry by co-precipitation. *Hydrometallurgy* **150**, 27–33. https://doi.org/10.1016/j.hydromet.2014.08.014 (2014).
22. Itakura, T., Sasai, R. & Itoh, H. Resource recovery from Nd–Fe–B sintered magnet by hydrothermal treatment. *Bull. Chem. Soc. Jpn.* **79**, 1303–1307. https://doi.org/10.1246/bcsj.79.1303 (2006).
23. Önal, M. A. R., Borra, C. R., Guo, M., Blanpain, B. & Van, G. T. Hydrometallurgical recycling of NdFeB magnets: Complete leaching, iron removal and electrolysis. *J. Rare Earths* **35**, 574–584. https://doi.org/10.1016/S1002-0721(17)60950-5 (2017).
24. Adachi, G., Shinozaki, K., Hirashima, Y. & Machida, K. Rare earth separation using chemical vapor transport with LnCl,-AlCl, gas phase complexes. *J. Less-Common Met.* **169**, L1–L4. https://doi.org/10.1016/0022-5088(91)90225-S (1991).
25. Gergoric, M., Ravaux, C., Steenari, B. M., Espegren, F. & Retegan, T. Leaching and recovery of rare-earth elements from neodymium magnet waste using organic acids. *Metals* **8**, 721–738. https://doi.org/10.3390/met8090721 (2018).
26. Baba, Y., Kubota, F., Kamiya, N. & Goto, M. Selective recovery of dysprosium and neodymium ions by a supported liquid membrane based on ionic liquids. *Solvent Extr. Res. Dev. Jpn.* **18**, 193–198. https://doi.org/10.15261/serdj.18.193 (2011).
27. Kim, T. A., Kang, M. C., Jung, G. B., Kim, D. S. & Yang, C. W. Novel method for preparing transmission electron microscopy samples of micrometer-sized powder particles by using focused ion beam. *Microsc. Microanal.* **23**, 1055–1060. https://doi.org/10.1017/S1431927617012557 (2017).
28. Park, S. M., Yoo, J. C., Ji, S. W., Yang, J. & Baek, K. Selective recovery of dissolved Fe, Al, Cu, and Zn in acid mine drainage based on modeling to predict precipitation pH. *Environ. Sci. Pollut. Res.* **22**, 3013–3022. https://doi.org/10.1007/s11356-014-3536-x (2015).
29. Paula A., Mónica C., Adriana S., Jorge T. & Denise E. Precipitation of Metals from Synthetic Laterite Nickel Liquor by Naoh. Hydroprocess, in *8th International Seminar on process Hydrometallergy* (2016).
30. Olena, O. & Serge, S. Investigation of FeCl$_3$ induced coagulation processes using electrophoretic measurement, nanoparticle tracking analysis and dynamic light scattering: importance of pH and colloid surface charge. *Colloids Surf. A Physicochem. Eng. Asp.* **461**, 212–219. https://doi.org/10.1016/j.colsurfa.2014.07.049 (2014).
31. Nwe, S., Lwin, T. S. & Kay, T. L. Study on extraction of lanthanum oxide from monazite concentrate. *Int. Sch. Sci. Res. Innov.* **2**(10), 226–229 (2008).
32. Liu, X. B. & Altounian, Z. The partitioning of Dy and Tb in NdFeB magnets: a first-principles study. *J. Appl. Phys.* **111**, 07A701.1-07A701.3. https://doi.org/10.1063/1.3670054 (2012).
33. Yu, N. J., Pan, N. J., Zhang, P. Y. & Ge, H. L. The origin of coercivity enhancement of sintered NdFeB magnets prepared by Dy addition. *J. Magn.* **18**(3), 235–239. https://doi.org/10.4283/JMAG.2013.18.3.235 (2013).

34. Li, W. F., Sepehri-Amin, H., Ohkubo, T., Hase, N. & Hono, K. Distribution of Dy in high-coercivity (Nd, Dy)–Fe–B sintered magnet. *Acta Mater.* **59**, 3061–3069. https://doi.org/10.1016/j.actamat.2011.01.046 (2011).
35. Tan, X., Parmar, X., Zhong, Y., Chaudhary, V. & Ramanujan, R. V. Effect of Dy substitution on the microstructure and magnetic properties of high (BH)max Nd-Dy-Fe-Co-B nanoparticles prepared by microwave processing. *J. Magn. Magn. Mater.* **471**, 278–285. https://doi.org/10.1016/j.jmmm.2018.09.017 (2019).
36. Wenlong, Y. *et al.* Influence of gadolinium on microstructure and magnetic properties of sintered NdGdFeB magnets. *J. Rare Earth* **30**, 133–136. https://doi.org/10.1016/S1002-0721(12)60009-X (2012).
37. Zhong, Y., Chaudhary, V., Tan, X., Parmar, H. & Ramanujan, R. V. High coercivity Dy substituted Nd-Fe-Co-B magnetic nanoparticles produced by mechanochemical processing. *Magn. Magn. Mater.* **475**, 554–562. https://doi.org/10.1016/j.jmmm.2018.08.061 (2019).
38. Rahimi, H., Ghasemi, A., Mozaffarinia, R. & Tavoosi, M. Coercivity enhancement mechanism in Dy-substituted Nd–Fe–B nanoparticles synthesized by sol–gel base method followed by a reduction diffusion process. *J. Magn. Magn. Mater.* **429**, 182–191. https://doi.org/10.1016/j.jmmm.2017.01.041 (2017).
39. Khan, I. & Hong, J. Electronic structure and magnetic properties of $Nd_2Fe_{14}B$. *J. Kor. Phys. Soc.* **68**, 1409–1414. https://doi.org/10.3938/jkps.68.1409 (2016).
40. Alam, A., Khan, M., McCallum, R. W. & Johnson, D. D. Site-preference and valency for rare-earth sites in $(R-Ce)_2Fe_{14}B$ magnets. *Appl. Phys. Lett.* **102**, 0424021–0424025. https://doi.org/10.1063/1.4789527 (2013).
41. Kitagawa, I. & Asari, Y. Magnetic anisotropy of $R2Fe14B$ (R=Nd, Gd, Y): Density functional calculation by using the linear combination of pseudo-atomic-orbital method. *Phys. Rev. B* **81**, 214408.1-214408.7. https://doi.org/10.1103/PhysRevB.81.214408 (2010).
42. Haider, S. K. *et al.* Determination of Dy substitution site in $Nd2−xDyxFe14B$ by HAADF-STEM and illustration of magnetic anisotropy of "g" and "f" sites, before and after substitution. *Sci. Rep.* **11**, 6347. https://doi.org/10.1038/s41598-021-85713-5 (2021).
43. Haider, S. K., Lee, J. Y., Pawar, A. U. *et al.* Novel eco-friendly low cost and energy efficient synthesis of $(Nd–Pr–Dy)_2Fe_{14}B$ magnetic powder from monazite concentrate. *Sci Rep.* **11**, 20594. https://doi.org/10.1038/s41598-021-99464-w (2021).
44. Haider, S. K., Ngo, H. M., Kim, D. *et al.* Enhancement of anisotropy energy of $SmCo_5$ by ceasing the coupling at 2c sites in the crystal lattice with Cu substitution. *Sci Rep.* **11**, 10063. https://doi.org/10.1038/s41598-021-89331-z (2021).
45. Butler, I. B., Schoonen, M. A. & Rickard, D. T. Removal of dissolved oxygen from water: a comparison of four common techniques. *Talanta* **41**, 211–215. https://doi.org/10.1016/0039-9140(94)80110-X (1994).

Acknowledgements

Author contributions

S.K.H. performed experiment did characterization and wrote manuscript. Y.S.K. helped in data interpretation and manuscript writing. D.K. helped in experiment and characterization.

Competing interests

The authors declare no competing interests.

Additional information

Supplementary Information The online version contains supplementary material available at https://doi.org/10.1038/s41598-021-01382-4.

Correspondence and requests for materials should be addressed to D.K. or Y.S.K.

Reprints and permissions information is available at www.nature.com/reprints.

Publisher's note Springer Nature remains neutral with regard to jurisdictional claims in published maps and institutional affiliations.